FINITE ELEMENT ANALYSIS OF QUANTUM STATES IN LAYERED QUANTUM SEMICONDUCTOR STRUCTURES WITH BAND NONPARABOLICITY EFFECT

Khai Q. Le
Department of Information Technology, Ghent University-IMEC, Sint-Pietersnieuwstraat 41, 9000 Ghent, Belgium; Corresponding author: ronaldokhai@yahoo.com

Received 24 April 2008

ABSTRACT: *A simultaneous calculation of eigenstates in the layered quantum semiconductor structures using the finite element method was developed. We proposed the approximation to linearize the nonlinear eigenvalue problem due to nonparabolicity effect and found the application range for the approach. The finite element calculation results showed an excellent agreement with the published results obtained by other authors. In addition, our calculated results confirm that the effect of nonparabolicity on the transition energy shift is considerably large for higher subbands and should be taken into account in the simulation and design of light emitters based on layered quantum semiconductor structures.* © 2008 Wiley Periodicals, Inc. Microwave Opt Technol Lett 51: 1–5, 2009; Published online in Wiley InterScience (www.interscience.wiley.com). DOI 10.1002/mop.23976

Key words: *band structure calculation; layered quantum semiconductor structures; quantum cascade lasers; nonparabolicity effect; finite element method*

1. INTRODUCTION

Quantum engineering of electronic energy states and wave functions using nanoscale layers of semiconductor compounds allows the design and the observation of quantum phenomena which are typically observed in atomic structures. Furthermore, the advances in growth technology of quantum well heterostructures have allowed tailoring of the optical and transport properties of semiconductor materials, resulting in a considerable increase in research activity directed toward the development of novel useful optoelectronic devices. One of the excellent examples of how quantum engineering can be used to devise efficient light emitters in mid-infrared to THz region is the quantum cascade (QC) laser [1]. To understand the physical properties of the heterostructure devices, one needs to solve the eigenvalue problem of carrier in the quantum well structure. However, the presence of the conduction band nonparabolicity effect (NPE) [2] makes it complicate. Under this effect, it becomes a nonlinear eigenvalue problem. Therefore, the problem in general cannot be solved exactly. The approximate calculation needs to be developed to find the close solution.

In addition, since the operating wavelength of and the carrier dynamics in the QC lasers are determined mainly by a quantum well structure rather than bandgaps of materials, an accurate theoretical modeling is very important in the QC laser design. There have been various methods used to calculate the band profiles in the quantum well structures, which include the matrix approach [3], the transfer matrix method [4], the finite difference method (FDM) [5, 6], and the finite element method (FEM) [7, 8]. The FDM and FEM are quite straightforward methods and advantageous in that all the subbands can be calculated simultaneously. However, this advantage of simultaneous calculation of all subbands hardly can be taken if the NPE is included. Thus, in the previous work, to include the NPE, subbands were calculated sequentially, and in each subband calculation, a good guess of an eigenenergy was to be made [9].

In our recent work [10], we proposed the new band structure calculation method based on the FDM, in which all subbands were calculated simultaneously even with taking into account the NPE. The key element of the new approach was the using of the first-order Taylor approximation of the energy dependency of the electron effective mass. With the proposed method, we have simultaneously calculated all the subband edge energy levels and the corresponding wave functions for QC laser structures. The finite difference calculation results showed good agreement with the previously reported results in specified range. However, in some cases of THz QC lasers [11] in which an accurate operating wavelength calculation is strongly required because of their low transition energy, a method more accurate than FDM may be required.

In this article, we present a more accurate approach sharing the same idea of using the first-order Taylor approximation of the energy dependency of the electron's effective mass to take into account the NPE. The method is based on the Galerkin's finite element procedure, and first-order line element is used for finite elements. The proposed method has been verified by being applied to calculate the conduction subband structures of the layered quantum semiconductor structures including the single quantum well with various well widths [8] as well as the previously reported QC lasers [12–16].

2. FORMULATION

2.1. Basic Equation

With the effective mass approximation, the envelope function ψ of an electron is obtained by solving the 1D Schrödinger equation:

$$-\frac{\hbar^2}{2}\frac{d}{dx}\left[\frac{1}{m^*(E,x)}\frac{d\psi(x)}{dx}\right]+V(x)\psi(x)=E\psi(x), \qquad (1)$$

where $V(x)$, E, $\psi(x)$, and $m^*(E,x)$ are the potential due to the external and the built-in electric field, eigenenergy, wave function corresponding to the eigenenergy E, and energy- and position-dependent electron effective mass, respectively. For a single quantum well, the energy-dependent electron effective masses in the well and the barrier including the effect of conduction band nonparabolicity are specifically given by [8]

$$m_w^*(E)=m_w^*\left(1+\frac{E}{E_w}\right), \qquad (2)$$

$$m_b^*(E)=m_b^*\left(1+\frac{E}{E_b}-\frac{V}{E_b}\right), \qquad (3)$$

where E_w , E_b , and V are the energy gaps between the conduction and the light-hole valence bands in the well and barrier materials, and the energy barrier height at the interfaces, respectively. The nonparabolicity coefficient is given by

$$\gamma_i=\frac{\hbar^2}{2m_i^*E_i}, (i=w,b). \qquad (4)$$

For a QC laser structure, the energy- and position-dependent electron effective mass with taking into account the NPE can be written as [17]

$$m^*(E,x)=m_b^*(x)\left(1+\frac{E}{E_g(x)}-\frac{V(x)}{E_g(x)}\right), \qquad (5)$$

where $m_b^*(x)$ and $E_g(x)$ are the effective mass of conduction band bottom and energy bandgap, respectively.

To take the advantage of the simultaneous calculation of all subbands, we propose the new approximation of the energy- and position-dependent effective electron mass based on the first-order Taylor approximation:

$$\frac{1}{m^*(E_i,x)} \cong \frac{1}{m_b^*(x)}\left[1 - \frac{E}{E_g(x)} + \frac{V(x)}{E_g(x)}\right] \text{ if } [E - V(x)] \ll E_g(x). \tag{6}$$

By substituting Eq. (6) into Eq. (1), we obtained

$$-\frac{\hbar^2}{2}\frac{d}{dx}\left\{\frac{1}{m_b^*(x)}\left[1 - \frac{E}{E_g(x)} + \frac{V(x)}{E_g(x)}\right]\frac{d\psi(x)}{dx}\right\} + V(x)\psi(x) = E\psi(x). \tag{7}$$

To reduce the number parameters, the coordinate x, the potential $V(x)$, the band gap $E_g(x)$, the electron effective mass $m_b^*(x)$, and the energy E are normalized as $\xi = x/L$, $V(\xi) = V(x)/E_1$, $E_g(\xi) = E_g(x)/E_1$, $m^*(\xi) = m_b^*(x)/m_b^*(0)$, and $\varepsilon = E/E_1$, respectively, where $E_1 = \hbar^2\pi^2/2m_b^*(0)L^2$ with the solution domain length of L, and $m_b^*(0)$ is the effective mass of the electron at $x = 0$. With this notation, the Schrödinger equation (7) is reduced to

$$-\frac{d}{d\xi}\frac{1}{m(\xi)}\frac{d\psi(\xi)}{d\xi} - \frac{d}{d\xi}\frac{V(\xi)}{m(\xi)E_g(\xi)}\frac{d\psi(\xi)}{d\xi} + \left[\frac{d}{d\xi}\frac{1}{m(\xi)E_g(\xi)}\frac{d\psi(\xi)}{d\xi} - \pi^2\psi(\xi)\right]\varepsilon + \pi^2 V(\xi)\psi(\xi) = 0. \tag{8}$$

2.2. Finite Element Method

We use the Galerkin's finite element procedure [18, 19] to solve Eq. (8). This equation could be reduced to [6]

$$\left(\psi_1\frac{1}{m_1}\frac{d\psi_1}{d\xi} - \psi_M\frac{1}{m_M}\frac{d\psi_M}{d\xi}\right) + \left(\psi_1\frac{V_1}{m_1E_{g1}}\frac{d\psi_1}{d\xi} - \psi_M\frac{V_M}{m_ME_{gM}}\frac{d\psi_M}{d\xi}\right) - \varepsilon\left(\psi_1\frac{1}{m_1E_{g1}}\frac{d\psi_1}{d\xi} - \psi_M\frac{1}{m_ME_{gM}}\frac{d\psi_M}{d\xi}\right) + ([P] + [S])\{\psi\} + \pi^2[Q]\{\psi\} = \varepsilon(\pi^2[R] + [H])\{\psi\}, \tag{9}$$

where

$$[P] = \sum_e \frac{1}{m_e}\int_e \frac{d[N_e]}{d\xi}\frac{d[N_e]^T}{d\xi}d\xi, \tag{10}$$

$$[S] = \sum_e \frac{V_e}{m_eE_{ge}}\int_e \frac{d[N_e]}{d\xi}\frac{d[N_e]^T}{d\xi}d\xi, \tag{11}$$

$$[H] = \sum_e \frac{1}{m_eE_{ge}}\int_e \frac{d[N_e]}{d\xi}\frac{d[N_e]^T}{d\xi}d\xi, \tag{12}$$

$$[Q] = \sum_e V_e\int_e [N_e][N_e]^T d\xi, \tag{13}$$

$$[R] = \sum_e \int_e [N_e][N_e]^T d\xi, \tag{14}$$

$$\{\psi\} = \sum_e \{\psi_e\}. \tag{15}$$

Assuming the Dirichlet condition ($\psi = 0$) or the Neumann condition ($d\psi/d\xi = 0$) at the leftmost Node 1 and the rightmost node M, we obtain from Eq. (9) the simple eigenvalue equation:

$$([P] + [S])\{\psi\} + \pi^2[Q]\{\psi\} = \varepsilon(\pi^2[R] + [H])\{\psi\}. \tag{16}$$

The above equation can be transformed into the following eigenvalue matrix equation:

$$[A]\{\psi\} = \varepsilon[B]\{\psi\}, \tag{17}$$

where [A] and [B] are the $N \times N$ symmetric and sparse matrixes (N is the total number of nodes), ε is an eigenvalue, and $\{\psi\} = [\psi_1,\psi_2,\ldots,\psi_N]^T$ is the corresponding eigenvector. Equation (17) is the matrix eigenvalue problem. There have been various methods developed to solve this kind of problem. Even some numerical libraries have been established. In this work, LAPACK++ package was used.

3. NUMERICAL RESULTS AND DISCUSSION

As shown previously, the approximation for the energy-dependent electron effective mass using the first-order Taylor expansion is only valid when the approximation condition is satisfied. Therefore, to verify the validity of our proposed approximation and find the application range of this approach, we have calculated the subband edge energies in the single quantum well for various well widths as well as the subband structure for various types of QC lasers and compared with those obtained by other authors.

We first calculated the subband edge energies of the single quantum well considered in [8]. The parameters used for the calculation of the subband edge energy using FEM are the same as in their work. In Table 1, the calculated subband edge energy E (meV) and the energy shift E_s due to the NPE are listed. It can be clearly seen that our results are in good agreement with values in the literature [8]. In a single quantum well, it is known that the energy shift due to the NPE becomes substantial for higher subband edge for large well widths.

TABLE 1 Well Width and Associated Eigenstate Energies and Energy Shifts From Nonparabolicity Versus Quantum Number of the Eigenstate

			$n = 1$	$n = 2$	$n = 3$	$n = 4$	$n = 5$
Well width (nm)							
5	E	FEM	80.31	256.14			
		Ref.	81.17	254.67			
	E_s	FEM	+1.47	−13.87			
		Ref.	+0.71	−11.33			
10	E	FEM	32.26	119.6	235.73		
		Ref	32.3	119.52	235.79		
	E_s	FEM	+0.7	−4.62	−22.22		
		Ref.	+0.7	−4.84	−22.87		
20	E	FEM	10.47	40.88	88.35	148.64	216.36
		Ref.	10.55	41.11	88.82	149.74	218.93
	E_s	FEM	+0.09	−0.56	−4.46	−14.61	−31.05
		Ref.	+0.19	−0.25	−3.81	−13.21	−28.22

TABLE 2 Material Parameters Used in the Calculation of the *GaAs/Al$_{0.33}$Ga$_{0.67}$As*-Based QC Laser

Material Parameters	*GaAs*	*Al$_{0.33}$Ga$_{0.67}$As*	*GaAs/Al$_{0.33}$Ga$_{0.67}$As*
Band offset ΔE_c (meV)	–	–	300
Effective mass	$0.0665m_o$	$0.094m_o$	–
Band gap (eV)	1.424	1.836	–

For the QC laser, to investigate the effect of nonparabolicity on energy shift and verify the validity of our FEM calculation, we have performed the subband structure calculation of various types of QC lasers with and without the NPE. We first investigated the application of the method to the *GaAs/Al$_{0.33}$Ga$_{0.67}$As*-based QC lasers proposed by Sirtori et al. [12] and Kruck et al. [13]. The material parameters of these structures are given in Table 2, while the calculated values [20] of the transition energy using FEM as well as FDM are listed in Tables 3 and 4. (The effect of doping concentration was ignored in all calculations. The bandgaps of materials are given in the work of Vurgaftman et al. [20].) The calculated wave functions are depicted in Figures 1 and 2, respectively. It can be clearly seen that the finite element analysis results are in excellent agreement with values presented in Ref. [12, 13] and provide closer estimation of the transition energies than our previous work using FDM. One can also see that the transition energy shift due to the NPE is small for the lower subbands, whereas it is considerably large for the higher subbands.

The proposed method is next applied to calculate the most common QC laser based on *Al$_{0.48}$In$_{0.52}$As* and *Ga$_{0.47}$In$_{0.53}$As* [14]. The material parameters of the structure are given in Table 5. The calculated wave functions are depicted in Figure 3. In Ref. [14], the authors reported the QC laser's experimental emission wavelength of $\lambda \approx 11.2\ \mu$m ($\Delta E_{32} = 110.7$ meV) and their theoretical calculated transition energy $\Delta E_{32} = 106.6$ meV. Our calculated transition energy using FEM with and without NPE are $\Delta E_{32} = 106.3$ meV and $\Delta E_{32} = 125.3$ meV, respectively. Our calculation including NPE is in good agreement with their calculation. Again, we can note that the NPE induces a considerable change in the transition energy of the QC lasers, and for an accurate modeling of QC lasers, NPE should be included.

Next, we calculated the subband structure for the QC laser based on AlAs and GaAs material which has a larger band offset. The material parameters of the structure are given in Table 6. The calculated laser transition energy reported by Becker et al. [15] is ΔE_{32} $= 109$ meV ($\lambda = 11.4\mu$m). Our calculated result with and without NPE are $\Delta E_{32} = 111.8$ meV and $\Delta E_{32} = 117.5$ meV, respectively. The band profiles and relevant wave functions of this QC laser are shown in Figure 4. It is clearly seen that our FEM calculation is also in very good agreement with the result obtained by Becker et al.

We now turn our attention to the THz QC laser structure proposed by Kumar et al. [16]. The material parameters of the structure are given in Table 7, while the calculated values of the transition energy and the band profile appear in Table 8 and Figure 5, respectively. Since the transition energy of THz QC lasers is quite low, an accurate theoretical calculation is strongly required in

TABLE 3 Calculated Transition Energy in the *GaAs/Al$_{0.33}$Ga$_{0.67}$As*-Based QC Laser [12]

	FEM			
Transition Energy (meV)	Without NPE	With NPE	FDM (with NPE)	Reference (with NPE)
ΔE_{21}	36.2	37.4	37	38
ΔE_{32}	147.2	135.2	129.5	134

TABLE 4 Calculated Transition Energy in the *GaAs/Al$_{0.33}$Ga$_{0.67}$As*-Based QC Laser [13]

	FEM			
Transition Energy (meV)	Without NPE	With NPE	FDM (with NPE)	Reference (with NPE)
ΔE_{32}	123.8	113.202	110.15	112
ΔE_{43}	78.7	56.984	56.63	58

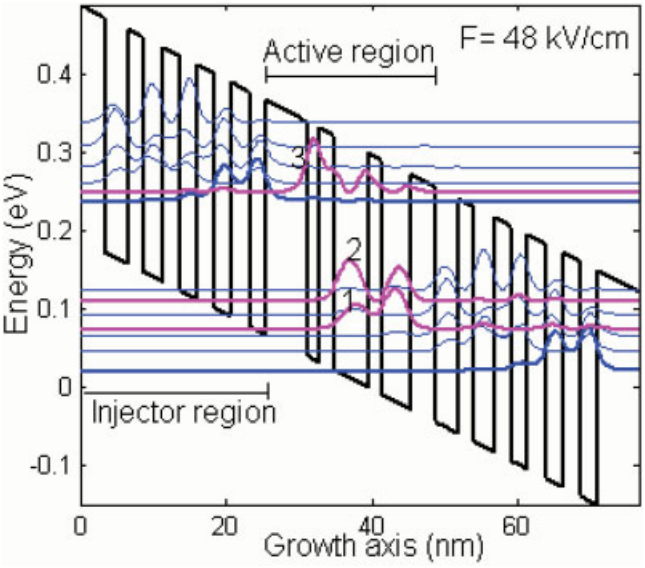

Figure 1 Schematic conduction band diagram of a portion of the *GaAs/Al$_{0.33}$Ga$_{0.67}$As*-based QC laser [12] under an electric field of 48 kV/cm. The solid curves represent the moduli squared of the relevant wave functions calculated by our FEM. [Color figure can be viewed in the online issue, which is available at www.interscience.wiley.com]

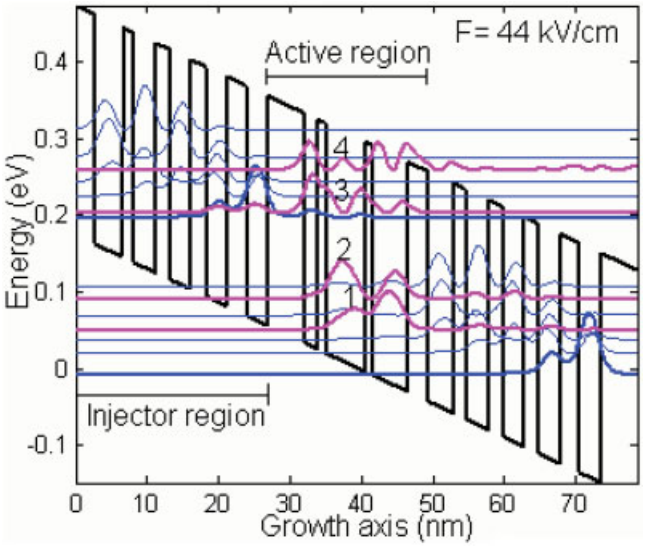

Figure 2 Schematic conduction band diagram of a portion of the *GaAs/Al$_{0.33}$Ga$_{0.67}$As*-based QC laser [13] under an electric field of 44 kV/cm. The solid curves represent the moduli squared of the relevant wave functions calculated by our FEM. [Color figure can be viewed in the online issue, which is available at www.interscience.wiley.com]

TABLE 5 Material Parameters Used in the Calculation of the $Al_{0.48}In_{0.52}As/Ga_{0.47}In_{0.53}As$-Based QC Laser

Material Parameters	$Ga_{0.47}In_{0.53}As$	$Al_{0.48}In_{0.52}As$	$Ga_{0.47}In_{0.53}As/Al_{0.48}In_{0.52}As$
Band offset ΔE_c (meV)	–	–	520
Effective mass	$0.043m_0$	$0.078m_0$	–
Band gap (eV)	0.75	1.45	–

the THz QC laser design. In that case, for determination of accurate transition energy, the FEM is expected to provide more accurate result than the FDM as seen in Table 8.

However, for the QC lasers based on the materials whose band parameters violate the approximation condition, the calculated results are incorrect. To prove this statement, we carried out the band structure calculation of the QC laser based on $Ga_{0.47}In_{0.53}As$ and $AlAs_{0.56}Sb_{0.44}$ [21]. In this work, authors reported the theoretical calculated transition energy $\Delta E_{32} = 435$ meV, while our FEM with and without NPE is 314.1 and 482.4 meV. The calculated wave functions are depicted in Figure 6.

The developed method was employed to calculate the subband structure of some common QC lasers based on various types of materials. The calculated results show an excellent agreement with those obtained by other authors where their band structure calculation were made by taking into account the NPE in different manner. From the calculation, we confirm that the transition energy shift due to the NPE is considerably large for the higher subbands, and for an accurate design of QC laser devices, the effect of nonparabolicity should be taken into account.

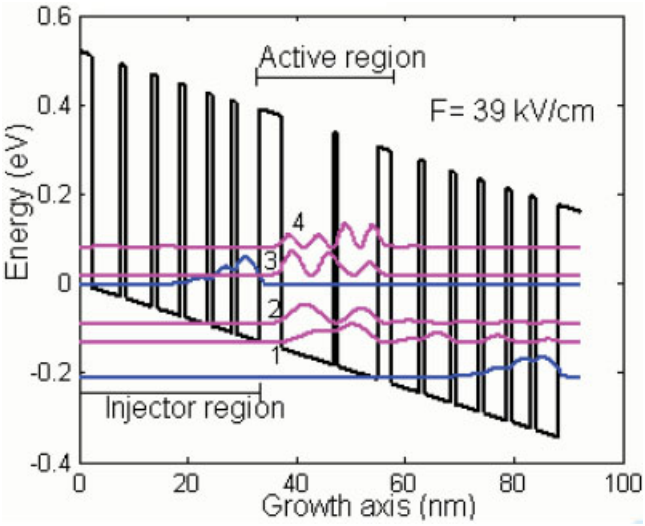

Figure 3 Schematic conduction band diagram of a portion of the $Al_{0.48}In_{0.52}As/Ga_{0.47}In_{0.53}As$-based QC laser [14] under an electric field of 39 kV/cm. The solid curves represent the moduli squared of the relevant wave functions calculated by our FEM. [Color figure can be viewed in the online issue, which is available at www.interscience.wiley.com]

TABLE 6 Material Parameters Used in the Calculation of the $GaAs/Al_{0.33}Ga_{0.67}As$-Based QC Laser

Material Parameters	$GaAs$	$AlAs$	$GaAs/AlAs$
Band offset ΔE_c (meV)	–	–	1000
Effective mass	$0.0665m_0$	$0.124m_0$	–
Band gap (eV)	1.424	2.4	–

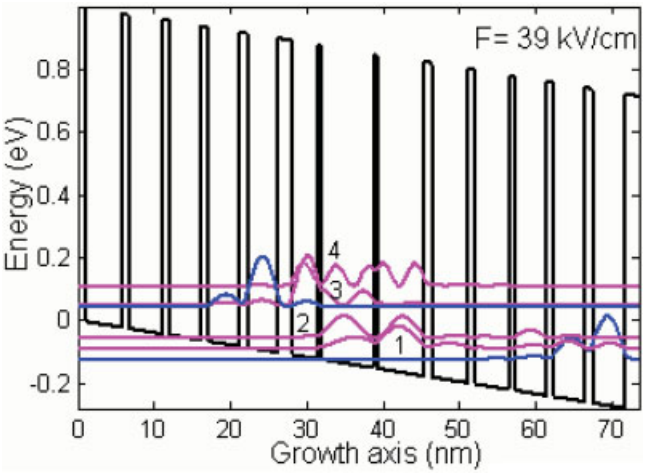

Figure 4 Schematic conduction band diagram of a portion of the $AlAs/GaAs$-based QC laser [15] under an electric field of 39 kV/cm. The solid curves represent the moduli squared of the relevant wave functions calculated by our FEM. [Color figure can be viewed in the online issue, which is available at www.interscience.wiley.com]

Up to now, we have been considering the eigenvalue problem where the presence of the NPE changes it to a nonlinear eigenvalue problem. Therefore, this work provides the approach to linearize the eigenvalue problem. As shown earlier, the approximation for the energy-dependent electron effective mass using the first-order Taylor expansion is only valid when the variable is small enough. By calculating the subband structure of the most common QC lasers, we found that this approach is valid for the QC lasers based on the materials where the direct conduction band discontinuity of the heterostructures must be smaller than the bandgap of each material ($\Delta E_c < E_g$).

4. CONCLUSIONS

A FEM has been established for the analysis of quantum states in single quantum well and various types of QC lasers. The proposed approximation of the energy-dependent electron effective mass shows an excellent agreement with previously reported results. We can simultaneously calculate all subband states of single quantum well and QC laser structures even including the conduction band NPE. We developed a numerical technique using the first-order Taylor expansion of the energy-dependent electron effective mass

TABLE 7 Material Parameters Used in the Calculation of the $GaAs/Al_{0.15}Ga_{0.85}As$-Based QC Laser

Material Parameters	$GaAs$	$Al_{0.15}Ga_{0.85}As$	$GaAs/Al_{0.15}Ga_{0.85}As$
Band offset ΔE_c (meV)	–	–	125.3
Effective mass	$0.0665m_0$	$0.079m_0$	–
Band gap (eV)	1.424	1.611	–

TABLE 8 Calculated Transition Energy in the $GaAs/Al_{0.15}Ga_{0.85}As$-Based QC Laser [16]

	FEM			
Transition Energy (meV)	Without NPE	With NPE	FDM With NPE	Reference With NPE
ΔE_{43}	9.0	7.8	7.1	7.7
ΔE_{21}	34.6	36.2	33.4	35.8

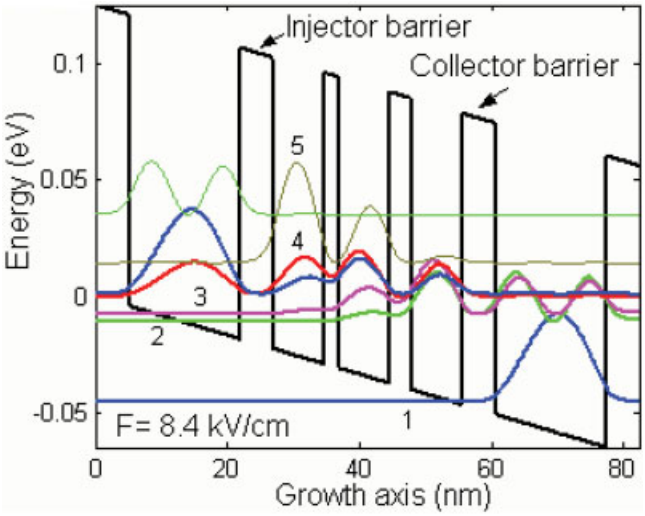

Figure 5 Schematic conduction band diagram of a portion of the $GaAs/Al_{0.15}Ga_{0.85}As$-based QC laser [16] under an electric field of 8.4 kV/cm. The solid curves represent the moduli squared of the relevant wave functions calculated by our FEM. [Color figure can be viewed in the online issue, which is available at www.interscience.wiley.com]

embedded in the FEM and applied it to various quantum well structures to verify its validity. Our calculations show good agreements with the previously reported results. The finite element calculated results also showed an obvious improvement compared to our previous work using FDM. Since all the bounded subbands in QC lasers can be simultaneously calculated with good accuracy using the proposed method, we believe that this method is very useful for QC laser design. Especially, for the QC lasers based on the bound-to-continuum structure [22] where many quantum states should be considered, the proposed method will provide a powerful design tool.

To improve the accuracy of the finite element analysis of eigenstates in QC lasers, we can apply the second or higher order line element for finite elements, which will be reported elsewhere.

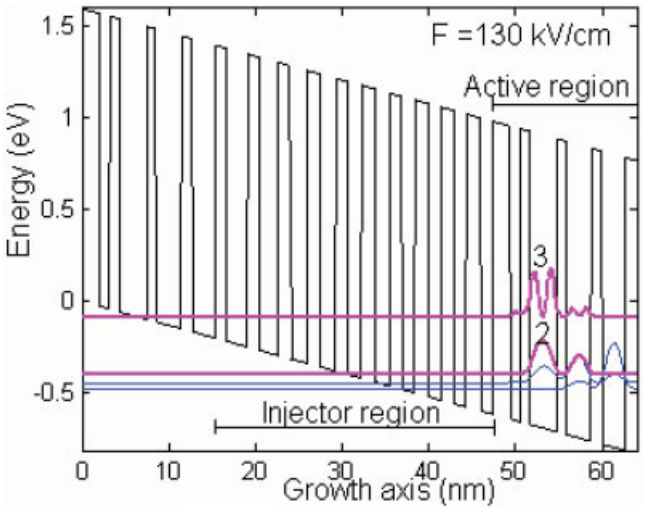

Figure 6 Schematic conduction band diagram of a portion of the $In_{0.53}Ga_{0.47}As/AlAs_{0.56}Sb_{0.44}$-based QC laser [21] under an electric field of 130 kV/cm. The solid curves represent the moduli squared of the relevant wave functions calculated by our FEM. [Color figure can be viewed in the online issue, which is available at www.interscience.wiley.com]

REFERENCES

1. J. Faist, F. Capasso, D.L. Sivco, A.L. Hutchinson, and A.Y. Cho, Quantum cascade laser, Science 64 (1994), 553–556.
2. D.F. Nelson, R.C. Miller, and D.A. Kleinman, Band nonparabolicity effects in semiconductor quantum wells, Phys Rev B 35 (1987), 7770.
3. A.K. Ghatak, K. Thyagarajan, and M.R. Shenoy, A novel numerical technique for solving the Schrodinger equation using matrix approach—Application to quantum well structures, IEEE J Quantum Electron 24 (1988), 1524.
4. B. Jonsson and S.T. Eng, Solving the Schrodinger equation in arbitrary quantum well potential profiles using the transfer matrix method, IEEE J Quantum Electron 26 (1990), 2025.
5. P. Harrison, Quantum wells, wires and dots: Theoretical and computational physics, 2nd ed., Wiley, Chichester, UK, 2005.
6. K. Kawano and T. Kitoh, Introduction to optical waveguide analysis—Solving Maxwell's equation and Schrödinger's equation, Wiley, New York, 2001, pp. 251-254.
7. K. Nakamura, A. Shimizu, M. Koshiba, and K. Hayata, Finite-element analysis of quantum wells of arbitrary semiconductors with arbitrary potential profiles, IEEE J Quantum Electron 25 (1989), 889.
8. H. Hayata, M. Koshiba, K. Nakamura, and A. Shimizu, Eigenstate calculation of quantum well structures using finite elements, Electron Lett 24 (1988), 614.
9. Y. Li, O. Voskoboynikov, C.P. Lee, and S.M. Sze, Computer simulation of electron energy levels for different shape InAs/GaAs semiconductor quantum dots, Comput Phys Commun 141 (2001), 66.
10. L.Q. Khai and S. Kim, A novel band structure calculation for the quantum cascade lasers with conduction band nonparabolicity effect, Presented at the 9th International Conference on Intersubband Transitions in Quantum Wells, Ambleside, Cumbria, UK.
11. R. Kohler, A. Tredicucci, F. Beltram, H.E. Beere, E.H. Linfield, A.G. Davies, D.A. Ritchie, R.C. Lotti, and F. Rossi, Terahertz semiconductor herterostructure laser, Nature 417 (2002), 156.
12. C. Sirtori, P. Kruck, S. Barbieri, O. Collot, J. Nagle, M. Beck, J. Faist, and U. Oesterle, $GaAs/Al_{0.33}Ga_{0.67}As$ quantum cascade lasers, Appl Phys Lett 73 (1998), 3486.
13. P. Kruck, H. Page, C. Sirtori, M. Stellmacher, and J. Nagle, Improved temperature performance of $GaAs/Al_{0.33}Ga_{0.67}As$ quantum cascade lasers with emission wavelength at $\lambda = 11\mu m$, Appl Phys Lett 76 (2000), 3340.
14. C. Sirtori, J. Faist, F. Capasso, D.L. Sivco, A.L. Hutchinson, and A.Y. Cho, Long wavelength infrared ($\lambda \approx 11\mu m$) quantum cascade lasers, Appl Phys Lett 69 (1996), 2810.
15. C. Becker, C. Sirtori, H. Page, G. Glastre, V. Ortiz, X. Marcadet, M. Stellmacher, and J. Nagle, AlAs/GaAs quantum cascade lasers based on large direct conduction band discontinuity, Appl Phys Lett 77 (2000), 463.
16. S. Kumar, B.S. Williams, Q. Hu, and J.L. Reno, 1.9 THz quantum cascade lasers with one-well injector, Appl Phys Lett 88 (2006), 121–123.
17. J. Bai and D.S. Citrin, Supersymmetric optimization of second harmonic generation in mid-infrared quantum cascade lasers, Opt Express 14 (2006), 4043.
18. K. Kawano and T. Kitoh, Introduction to optical waveguide analysis—Solving Maxwell's equation and Schrödinger's equation, Wiley, New York, 2001, pp. 254–260.
19. O.C. Zienkiewics, The finite element method, 3rd ed., McGraw-Hill, New York, 1997.
20. Vurgaftman et al., J Appl Phys 89 (2001), 5815.
21. C.A. Evans, V.D. Jovanovic, D. Indjin, Z. Ikonik, and P. Harrison, Design and simulation of InGaAs/AlAsSb quantum-cascade lasers for short wavelength emission, Appl Phys Lett 87 (2005), 141–109.
22. J. Faist, D. Hofstetter, M. Becke, T. Aellen, M. Rochat, and S. Blaser, Bound-to-continuum and two-phonon resonance quantum-cascade lasers for high duty cycle, high-temperature operation, IEEE J Quantum Electron 38 (2002), 533.